



PERGAMON

Journal of the Mechanics and Physics of Solids
50 (2002) 1547–1564

JOURNAL OF THE
MECHANICS AND
PHYSICS OF SOLIDS

www.elsevier.com/locate/jmps

Intersonic crack propagation in homogeneous media under shear-dominated loading: theoretical analysis

Dhirendra V. Kubair^{a,b}, Philippe H. Geubelle^{a,b,*},
Yonggang Y. Huang^c

^a*Department of Aeronautical and Astronautical Engineering, MC 236, University of Illinois at Urbana-Champaign, 306 Talbot Lab.; 104 South Wright Street, Urbana, IL 61801, USA*

^b*Center for the Simulation of Advanced Rockets, University of Illinois at Urbana-Champaign, 306 Talbot Lab.; 104 South Wright Street, Urbana, IL 61801, USA*

^c*Department of Mechanical and Industrial Engineering, University of Illinois at Urbana-Champaign, 306 Talbot Lab.; 104 South Wright Street, Urbana, IL 61801, USA*

Received 6 June 2001; accepted 29 January 2002

Abstract

The mechanics of cohesive failure under mixed-mode loading is investigated for the case of a steadily propagating subsonic and intersonic dynamic crack subjected to a follower tensile and shear distributed load. The cohesive failure model chosen in this study is rate independent but accounts for the coupling between normal and tangential damage. Special emphasis is placed here on mixed-mode cases with predominantly shear loading. The analysis shows that the size of the mixed-mode cohesive zone is smaller than that obtained in the pure shear case. The relative extent of the shear and tensile cohesive damage zones depends on the crack speed and the mode mixity. In the intersonic regime, the failure process takes place exclusively in shear, even under remote mixed-mode loading conditions. © 2002 Published by Elsevier Science Ltd.

Keywords: A. Dynamic fracture; B. Elastic material; C. Boundary integral equations

1. Introduction

In a recent article, Geubelle and Kubair (2001) have presented the results of a numerical analysis of the intersonic motion of a planar crack (i.e., for which the crack

* Corresponding author. Tel.: +1-217-244-7648; fax: +1-217-244-0720.
E-mail address: geubelle@uiuc.edu (P.H. Geubelle).

speed exceeds the shear wave speed c_s but remains below the dilatational wave speed c_d of the surrounding medium) embedded in a linearly elastic solid and subjected to shear-dominated loading conditions. This study, which was motivated by direct observations of intersonic crack propagation in homogeneous isotropic media (Rosakis et al., 1999; Ravi-Chandar et al., 2000), was conducted with the aid of a special form of the elastodynamic boundary integral scheme referred to as the spectral scheme (Geubelle and Rice, 1995; Breitenfeld and Geubelle, 1998), combined with a cohesive failure model used to capture the spontaneous initiation and propagation the crack.

In addition to shedding some light on the transition between subsonic and intersonic regimes, this numerical study showed that intersonic crack propagation was possible under mixed-mode loading conditions. In particular, it showed that, under well established (quasi steady-state) intersonic conditions, the failure appears to take place exclusively in shear, despite the fact that the far-field loading conditions have a tensile component. Normal opening of the crack was detected only after the completion of the cohesive failure process. This result reinforced early theoretical analyses indicating that intersonic crack propagation is physically impossible under tensile (mode I) loading because, under these conditions, energy is not absorbed by but emanates from the crack tip region (Freund, 1990). A direct consequence of the shear nature of the failure process is the fact that intersonic motion under mixed-mode conditions is achieved when the shear traction component applied along the fracture plane reaches a critical fraction of the material strength that can give rise to pure shear intersonic crack propagation speeds.

The issue of mixed-mode cohesive failure under both subsonic and intersonic conditions is revisited in this paper for the special case of steady-state crack propagation. We present a detailed analytical study of the steady-state propagation of a semi-infinite crack subjected to a follower distributed load, using the same coupled quasi-linear cohesive failure model used in the aforementioned numerical transient analysis performed by Geubelle and Kubair (2001). Special emphasis is placed here on the effect of the crack speed on the relative importance of shear and tensile failure processes taking place in the vicinity of the advancing crack front. After a description of the fracture problem and of its mathematical formulation (Section 2), we successively summarize the pure mode II (Section 3) and mixed-mode (Section 4) solutions for both the subsonic and intersonic regimes.

The present analytical study builds on various theoretical investigations on steady-state propagation in the subsonic and intersonic regimes. Analysis of a pure shear steady-state propagation at intersonic speeds were performed by Burridge (1973), Burridge et al. (1979) and Freund (1979), who showed that with a singular crack model only one intersonic speed is possible. Their work also showed that the entire intersonic regime of propagation was possible by considering a finite-size cohesive zone trailing the crack tip. Similar analyses on self-similar mode 2 crack propagation have been performed by Broberg (1980, 1989) in which the near tip field has been derived. Gao et al. (1999) and Huang and Gao (2001, 2002) have considered singular crack models in their pure shear intersonic crack propagation analysis in a homogeneous media. In a recent work, Samudrala and co-workers (2002) have analyzed intersonic crack

propagation in isotropic media subjected to pure mode 2 loading, in which they have studied the effect of including rate dependence in the friction law.

2. Problem description and solution

2.1. Problem description

The steady-state dynamic fracture problem studied hereafter is presented in Fig. 1. It consists of a semi-infinite crack propagating at a constant velocity v_c along the $x_2 = 0$ plane, in the positive x_1 -direction. Both subsonic ($v_c < c_s$) and intersonic ($c_s < v_c < c_d$) regimes of propagation are considered in our analysis. The crack is subjected to a uniformly distributed mixed-mode follower load over a portion L behind the tip of the cohesive zone and the length of the cohesive zone is L_c . With the steady-state assumption, the moving crack tip coordinates can be related to the fixed coordinate system as $(x_1, x_2) = (X - v_c t, Y)$, where (x_1, x_2) are the crack tip coordinates, (X, Y) are the stationary coordinates and t is the time. The in-plane displacements can be written in terms of the Helmholtz potentials (ϕ, ψ) as

$$u_1 = \phi_{,1} + \psi_{,2}, \quad u_2 = \phi_{,2} - \psi_{,1}, \tag{1}$$

where $(\cdot)_{,x} = \partial(\cdot)/\partial x_x$.

The momentum balance equations take the form

$$\alpha_d^2 \phi_{,11} + \phi_{,22} = 0, \quad \alpha_s^2 \psi_{,11} + \psi_{,22} = 0. \tag{2}$$

Here, α_s and α_d are defined as

$$\alpha_s^2 = 1 - \left(\frac{v_c}{c_s}\right)^2, \quad \alpha_d^2 = 1 - \left(\frac{v_c}{c_d}\right)^2, \tag{3}$$

where $c_s = \sqrt{\mu/\rho}$ is the shear wave speed and $c_d = \sqrt{(\kappa + 1)/(\kappa - 1)}c_s$ is the dilatational wave speed, with $\kappa = 3 - 4\nu$ in plane strain, $\kappa = (3 - \nu)/(1 + \nu)$ in plane stress, μ is the shear modulus and ρ the material density. Eqs. (2) can be solved by the method of characteristics. The characteristics of the first equation are complex $\forall v_c \in [0, c_d]$ and

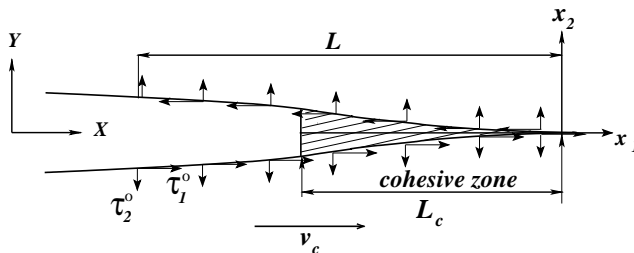


Fig. 1. Geometry of the mixed-mode steady-state propagation problem.

given by $z_d = x_1 \pm i\alpha_d x_2$ ($i^2 = -1$). The characteristics of the second equation are complex for $v_c < c_s$ ($\alpha_s^2 > 0$) and real for $v_c > c_s$ ($\alpha_s^2 < 0$), and are given by $z_s = x_1 \pm i\alpha_s x_2$. A general solution to (2) is thus given by

$$\begin{aligned} \phi &= \Re[F(z_d)] \quad \forall v_c \in [0, c_d], \\ \psi &= \begin{cases} \Im[G(z_s)] & \forall v_c \in [0, c_s], \\ g(z_s) & \forall v_c \in [c_s, c_d], \end{cases} \end{aligned} \tag{4}$$

where \Re and \Im stand for real and imaginary parts of a complex argument, respectively. $F(z_d)$, $G(z_s)$ are analytic functions, analytic everywhere except on the crack plane and $g(z_s)$ is a real function.

The displacements and stresses in the subsonic regime can be expressed as

$$\begin{aligned} u_1 &= \Re[F'(z_d) + |\alpha_s|G'(z_s)], \\ u_2 &= -\Im[\alpha_d F'(z_d) + G'(z_s)], \\ \sigma_{11} &= \mu \Re[(1 + 2\alpha_d^2 - \alpha_s^2)F''(z_d) + 2|\alpha_s|G''(z_s)], \\ \sigma_{22} &= -\mu \Re[(1 + \alpha_s^2)F''(z_d) + 2|\alpha_s|G''(z_s)], \\ \sigma_{12} &= -\mu \Im[2\alpha_d F''(z_d) + (1 + \alpha_s^2)G''(z_s)]. \end{aligned} \tag{5}$$

In the intersonic regime, they take the form

$$\begin{aligned} u_1 &= \Re[F'(z_d)] + |\alpha_s|g'(z_s), \\ u_2 &= -\alpha_d \Im[F'(z_d)] - g'(z_s), \\ \sigma_{11} &= \mu \{ (1 + 2\alpha_d^2 - \alpha_s^2) \Re[F''(z_d)] + 2|\alpha_s|g''(z_s) \}, \\ \sigma_{22} &= -\mu \{ (1 + \alpha_s^2) \Re[F''(z_d)] + 2|\alpha_s|g''(z_s) \}, \\ \sigma_{12} &= -\mu \{ 2\alpha_d \Im[F''(z_d)] + (1 + \alpha_s^2)g''(z_s) \}. \end{aligned} \tag{6}$$

As summarized in the following sections, the functions F , G and g are determined with the aid of the method described by Freund (1990) by using either the mode 1 or mode 2 symmetry along with the traction boundary conditions on the fracture plane. In both subsonic (Section 2.2) and intersonic (Section 2.3) regimes, the mixed-mode problem is then solved by combining the mode 1 and mode 2 solutions.

2.2. Subsonic regime

2.2.1. Mode 1

Mode 1 symmetry implies that $\sigma_{12}(x_1, x_2 = 0) = 0 \quad \forall x_1 \in [-\infty, \infty]$, from which we obtain

$$G'' = \frac{-2\alpha_d}{(1 + \alpha_s^2)} F''. \tag{7}$$

Further, setting $F''_+ = \bar{F}''_-$, with $F''_{\pm} = F''(x_1, x_2 = 0^{\pm})$ and \bar{F} denoting the complex conjugate of F , the normal stress on $x_2 = 0$ plane can be written as

$$\sigma_{22}(x_1, 0) = \mu \frac{(4\alpha_s\alpha_d - (1 + \alpha_s^2)^2) F''_+ - F''_-}{(1 + \alpha_s^2)} \tag{8}$$

Let $\tau_2(x_1)$ denote the normal cohesive traction acting inside the cohesive zone of length L_{c2} . Solving (8) for F'' leads to following relation between δ'_2 and τ_2 :

$$\delta'_2(x_1) = \frac{2\alpha_d(1 - \alpha_s^2)}{(4\alpha_s\alpha_d - (1 + \alpha_s^2)^2)} \frac{1}{\mu\pi} \left[\int_{L_{c2}} \left(\frac{\eta}{x_1}\right)^{1/2} \frac{\tau_2(\eta)}{(x_1 - \eta)} d\eta + \frac{P_2(x_1)}{x_1^{1/2}} \right], \tag{9}$$

while the normal stress on the crack plane takes the form

$$\sigma_{22}(x_1, x_2 = 0) = \frac{1}{\pi} \left[\int_{L_{c2}} \left(\frac{\eta}{x_1}\right)^{1/2} \frac{\tau_2(\eta)}{(x_1 + \eta)} d\eta + \frac{P_2(x_1)}{x_1^{1/2}} \right]. \tag{10}$$

To obtain a solution, we need to supplement the above equations with a cohesive zone law describing the evolution of the cohesive traction τ_2 during the failure process. In the present study, a coupled, damage-dependent, but rate-independent law is used and is presented later in this section. In (10), $P_2(x_1)$ denotes some general traction applied on the crack faces. The expression of P_2 for a constant magnitude follower load τ_2^0 applied on the crack faces up to a length L behind the cohesive zone tip (Fig. 1) is

$$P_2(x_1) = \int_L \frac{\tau_2^0 \sqrt{\eta}}{x_1 - \eta} d\eta. \tag{11}$$

The length of the cohesive zone under pure mode 1 loading is then determined by satisfying the Dugdale condition ($\delta'_2(x_1 = 0) = 0$):

$$P_2(x_1 = 0) = \int_{L_{c2}} \frac{\tau_2(\eta)}{\eta^{1/2}} d\eta. \tag{12}$$

2.2.2. Mode 2

The pure mode 2 solution is obtained in a very similar way, starting from the condition $\sigma_{22}(x_1, x_2 = 0) = 0 \forall x_1 \in [-\infty, \infty]$ which yields

$$G'' = \frac{-(1 + \alpha_s^2)}{2\alpha_s} F''. \tag{13}$$

By setting $F''_+ = -\bar{F}''_-$, the shear stress on the $x_2 = 0$ plane can be written as

$$\sigma_{12}(x_1, 0) = \mu \frac{(4\alpha_s\alpha_d - (1 + \alpha_s^2)^2) F''_+ - F''_-}{(2i\alpha_s)} \tag{14}$$

leading to the following relation between the slope of the sliding displacement δ'_1 and the shear cohesive traction τ_1 acting inside the cohesive zone of length L_{c1}

$$\delta'_1(x_1) = \frac{2\alpha_s(1 - \alpha_s^2)}{(4\alpha_s\alpha_d - (1 + \alpha_s^2)^2)} \frac{1}{\mu\pi} \left[\int_{L_{c1}} \left(\frac{\eta}{x_1}\right)^{1/2} \frac{\tau_1(\eta)}{(x_1 - \eta)} d\eta + \frac{P_1(x_1)}{x_1^{1/2}} \right]. \tag{15}$$

The shear stress on the crack plane can then be written as

$$\sigma_{12}(x_1, x_2 = 0) = \frac{1}{\pi} \left[\int_{L_{c1}} \left(\frac{\eta}{x_1} \right)^{1/2} \frac{\tau_1(\eta)}{(x_1 + \eta)} d\eta + \frac{P_1(x_1)}{x_1^{1/2}} \right], \tag{16}$$

where $P_1(x_1)$ denotes some general shear traction applied on the crack faces and is equal to

$$P_1(x_1) = \int_L \frac{\tau_1^0 \sqrt{\eta}}{x_1 - \eta} d\eta \tag{17}$$

for the mode 2 follower load problem described in Fig 1.

Closed-form solution to the pure mode cases can be obtained for a spatially dependent cohesive law as described in Appendix A.

2.2.3. Mixed mode

As indicated earlier, the solution to the mixed-mode case is obtained by combining the pure mode solutions described by (9) and (15). An expression relating the slope of displacement jump (δ'_α) and stress ($\sigma_{\alpha 2}$) to the cohesive tractions (τ_α) and external applied loads (P_α) can be written as

$$\begin{aligned} \frac{\delta'_\alpha}{C_\alpha(v_c)} &= \frac{1}{\pi\mu} \int_{L_{c\alpha}} \left(\frac{\eta}{x_1} \right)^{q_\alpha} \frac{\tau_\alpha}{(x_1 - \eta)} d\eta + \frac{P_\alpha}{\pi\mu}. \\ \sigma_{\alpha 2} &= \frac{1}{\pi} \int_{L_{c\alpha}} \left(\frac{\eta}{x_1} \right)^{q_\alpha} \frac{\tau_\alpha}{(x_1 + \eta)} d\eta + \frac{P_\alpha}{\pi}. \end{aligned} \tag{18}$$

(no sum on α)

In (18), the constants $C_\alpha(v_c)$ and order of singularities q_α are given by

$$\begin{aligned} C_1(v_c) &= \frac{2\alpha_s(1 - \alpha_s^2)}{[4\alpha_s\alpha_d - (1 + \alpha_s^2)^2]}, \quad q_1 = \frac{1}{2}, \\ C_2(v_c) &= \frac{2\alpha_d(1 - \alpha_s^2)}{[4\alpha_s\alpha_d - (1 + \alpha_s^2)^2]}, \quad q_2 = \frac{1}{2} \end{aligned} \tag{19}$$

and are shown in Fig. 2. The mode mixity of the applied load is denoted by the angle γ as in

$$Pe^{i\gamma} = P_2 + iP_1. \tag{20}$$

i.e., $\gamma=0^\circ$ and 90° corresponds to pure mode 1 and mode 2, respectively. The coupling between the integro-differential equations (18) is associated with the form of the cohesive law describing the failure process under mixed-mode conditions. In the present study, we use the coupled, rate-independent, quasi-linear cohesive law, as we did in the related numerical analysis (Geubelle and Kubair, 2001) and is given by

$$\tau = \frac{\tau_\alpha}{\tau_\alpha^c} = \left\langle 1 - \sqrt{\left(\frac{\delta_1}{\delta_1^c} \right)^2 + \left(\frac{\delta_2}{\delta_2^c} \right)^2} \right\rangle \tag{21}$$

(no sum on α),

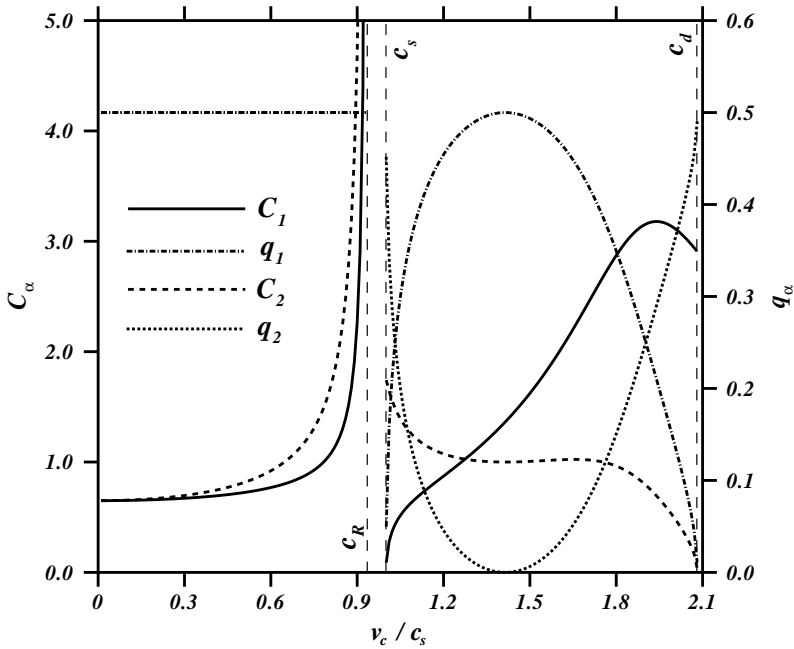


Fig. 2. Velocity dependence of the coefficients C_α and power of singularity q_α defined by (19), (28) and (32) for a Poisson's ratio of $\nu = 0.35$. Values of C_α in the range of $c_R < v_c < c_s$ are negative and are not shown. In the intersonic regime, only the mode 2 solution exhibits singularity.

where τ_α^c denotes the initial tangential ($\alpha = 1$) and normal ($\alpha = 2$) strengths of the material and $\langle \Phi \rangle$ is equal to Φ for $\Phi > 0$ and zero otherwise. In Eq. (21), δ_α^c are the critical values of the normal ($\alpha = 2$) and tangential ($\alpha = 1$) displacement jumps. The Dugdale condition at the cohesive zone tip then yields

$$\frac{C_1(v_c)\tau_1^c}{\sin(\gamma)} \int_0^{L_{c_1}} \frac{\tau(\xi)}{\sqrt{\xi}} d\xi = \frac{C_2(v_c)\tau_2^c}{\cos(\gamma)} \int_0^{L_{c_2}} \frac{\tau(\eta)}{\sqrt{\eta}} d\eta, \tag{22}$$

where, as before, L_{c_1} and L_{c_2} denote the extent of the shear and tensile failure taking place inside the cohesive zone ahead of the crack tip, respectively. Normalizing the above equation with the mixed-mode cohesive zone length the cohesive zone given by $\tau(L_c) = 0$, we get

$$\frac{\alpha_s}{\alpha_d} \frac{1}{\tan(\gamma)} = \frac{\int_0^\Gamma \frac{\tau(\eta)}{\sqrt{\eta}} d\eta}{\int_0^1 \frac{\tau(\xi)}{\sqrt{\xi}} d\xi}, \tag{23}$$

where $\Gamma = L_{c_2}/L_c \leq 1$ is the ratio of the tensile cohesive zone to the length of the cohesive zone for predominantly shear loading. A closed-form expression for Γ is possible for the case of a spatially dependent cohesive law as summarized in Appendix B.

For the damage-dependent cohesive law defined in Eq. (21), an iterative solution scheme such as that described in Section 3 is required.

2.3. Intersonic case

2.3.1. Mode 1

The mode 1 symmetry condition can be used to obtain an expression for the real function $g(x_1)$

$$g''(x_1) = \frac{-2i\alpha_d}{(1 + \alpha_s^2)} \frac{1}{2} [F''(x_1) - \bar{F}''(x_1)]. \tag{24}$$

Defining

$$A = 4|\alpha_s|\alpha_d, \quad B = (1 + \alpha_s^2)^2, \tag{25}$$

the normal stress σ_{22} on the crack plane ($x_2 = 0$) can be written as

$$\frac{-2\alpha_d}{\mu[B + iA]} \sigma_{22}(x_1, 0) = F''_+ - \left[\frac{B - iA}{B + iA} \right] F''_-. \tag{26}$$

The resulting Cauchy singular equation between the slope of the crack opening displacement δ'_2 to the cohesive traction τ_2 present inside the cohesive zone, under the effect of an external applied load P_2 , takes the form

$$\delta'_2(x_1) = \frac{-C_2(v_c)}{\pi} \frac{1}{\mu} \cos(\pi q_2(v_c)) \left\{ \int_{L_{c_2}} \left(\frac{\eta}{x_1} \right)^{-q_2(v_c)} \frac{\tau_2(\eta)}{(\eta - x_1)} d\eta + \frac{P_2(x_1)}{x_1^{-q_2(v_c)}} \right\} - \frac{C_2(v_c)}{\mu} \sin(\pi q_2(v_c)) \{ \tau_2(x_1) + P_2(x_1) \}, \tag{27}$$

where $C_2(v_c)$ is a non-dimensional premultiplier and $q_2(v_c)$ is the mode 1 order of singularity given by

$$C_2(v_c) = \frac{2(1 + \alpha_s^2)}{4\alpha_s} \sin(\pi q_2(v_c)),$$

$$q_2(v_c) = \frac{1}{\pi} \tan^{-1} \left[\frac{A}{B} \right] \tag{28}$$

and are shown in Fig. 2, as a function of the crack speed. Analysis of the mode 1 equations shows that the solution of the above integral equation leads to a physically unrealistic negative cohesive zone length ($L_{c_2} < 0$).

2.3.2. Mode 2

In the mode 2 case, the real function $g(x_1)$ takes the form

$$g''(x_1) = \frac{-(1 + \alpha_s^2)}{2|\alpha_s|} \frac{1}{2} [F''(x_1) + \bar{F}''(x_1)]. \tag{29}$$

The shear stress σ_{12} on the crack plane can be written as

$$\frac{-2(1 + \alpha_s^2)^2}{\mu[A - iB]} \sigma_{12}(x_1, 0) = F''_+ - \left[\frac{A + iB}{A - iB} \right] F''_- \tag{30}$$

leading to the relation

$$\delta'_1(x_1) = \frac{C_1(v_c)}{\pi} \frac{1}{\mu} \sin(\pi q_1(v_c)) \left\{ \int_{L_{c_1}} \left(\frac{\eta}{x_1} \right)^{q_1(v_c)} \frac{\tau_1(\eta)}{(\eta - x_1)} d\eta + \frac{P_1(x_1)}{x_1^{q_1(v_c)}} \right\} + \frac{C_1(v_c)}{\mu} \cos(\pi q_1(v_c)) \{ \tau_1(x_1) + P_1(x_1) \}, \tag{31}$$

where the non-dimensional premultiplier $C_1(v_c)$ and mode 2 order of singularity $q_1(v_c)$ are given by

$$C_1(v_c) = \frac{2(1 + \alpha_s^2)}{4\alpha_d} \sin(\pi q_1(v_c)),$$

$$q_1(v_c) = \frac{1}{\pi} \tan^{-1} \left[\frac{B}{A} \right] \tag{32}$$

and are shown in Fig. 2. The length of cohesive zone L_{c_1} is evaluated by satisfying the Dugdale condition

$$P_1(x_1 = 0) = \int_{L_{c_1}} \frac{\tau_1(\eta)}{\eta^{(1-q_1(v_c))}} d\eta. \tag{33}$$

2.3.3. Mixed mode

The mixed-mode solution in the intersonic regime is obtained by combining the two pure mode solutions. As seen from the pure mode results, a mode 1 crack becomes a radiating source in the intersonic regime, thereby preventing tensile cohesive damage. Therefore, since there can be no tensile damage inside the cohesive zone, the mixed-mode problem is decoupled for intersonic speeds. The solution to the mixed-mode problem is obtained by first obtaining the shear solution using Eq. (31). The crack opening (δ_2) behind the crack tip is then calculated by solving the integral Eq. (27), which completes the solution of the mixed-mode problem. A numerical scheme is required to obtain a solution to the mixed-mode problem as the chosen cohesive zone law (21) is damage dependent. The algorithm used to solve the equations is presented in the next section.

2.4. Numerical solution of the governing equations

The equation for the slope of the displacement jump is given by a Cauchy singular equation of the first kind. The Gauss–Legendre quadrature scheme is used to solve the governing singular integral equation (Erdogan et al., 1973). For example, in Eq. (18), x_1 and η are chosen as $x_1 = (1 - s)/2$ and $\eta = (1 - r)/2$, with s and r being the ones and zeros of the Chebyshev’s polynomial. Along with the quadrature scheme, Picard’s iteration scheme is used to solve the integro-differential equations, which, in this work, have the form

$$\delta'_{\beta}(x_1) = \frac{C_{\beta}}{\pi} \int_{L_{c_{\beta}}} \left(\frac{\eta}{x_1} \right)^{q_{\beta}} \tau_{\beta}(\delta_x(\eta)) \frac{d\eta}{(x_1 - \eta)} + \frac{f_{\beta}(x_1)}{x_1^{q_{\beta}}} \quad (\text{no sum on } \beta). \tag{34}$$

The iterative scheme can be summarized as follows:

1. Guess an initial distribution of the normal and tangential displacement jumps $\delta_\alpha(x_1)$ inside the cohesive zone;
2. Compute $\tau_\beta(\delta_\alpha)$ by Eq. (21);
3. Obtain δ'_β by integrating Eq. (34) using the Gauss–Legendre quadrature scheme;
4. Integrate δ'_β to obtain δ_β ;
5. In the subsonic regime, compute Γ (Eq. (23)) using the current value of τ_α ;
6. Check for convergence by computing the error norm $\varepsilon = \|\delta_\alpha^N - \delta_\alpha^{N-1}\|$ for the N th iteration;
7. If $\varepsilon > \text{Tol}$, go back to Step 2;

In the present study, a tolerance (Tol) of 10^{-6} was used and convergence was achieved in a maximum of 10 iterations.

3. Pure mode crack propagation

The steady-state solution for the pure mode cases is available in the literature both in the subsonic and intersonic regimes (Burrige et al., 1979; Broberg, 1980; Freund, 1990). In this section, results for the pure mode cases are presented for the sake of completeness and to contrast them with the mixed-mode solutions described in Section 4. As in our numerical simulations (Geubelle and Kubair, 2001), properties of Homalite were chosen in solving the governing equations: shear modulus $\mu = 1962.5$ MPa, Poisson's ratio $\nu = 0.35$ and density $\rho = 1230$ kg/m³, resulting in a plane-strain dilatational wave speed $c_d = 2360$ m/s and a shear wave speed $c_s = 1263$ m/s. For simplicity, the fracture properties inside the cohesive zone are assumed to be equal under both tensile (mode 1) as well as shear (mode 2) failure. The initial cohesive strength τ^c was assumed to be 5 MPa.

For a rate-independent cohesive model such as that used in the present study, the velocity dependence of the solution is only associated with the pre-multipliers C_α and the orders of singularity q_α entering Eqs. (9), (15), (27) and (31). The parameters C_α and q_α appearing in the pure mode 1 and mode 2 solutions have been shown in Fig. 2 as a function of the crack speed. In the subsonic regime, the stress singularity is constant and is equal to $1/2$ in both mode 1 and mode 2 cases. In the intersonic regime, only the mode 2 field is singular ($0 \leq q_1 \leq 1/2$), since $q_2 = q_1 - 1/2$, the tensile field is non-singular. As the value of the pre-multiplier C_1 and the stress singularity q_1 are identical at $v_c = 0.698c_s$ and $\sqrt{2}c_s$, the solution under pure mode 2 loading for a rate-independent cohesive law is identical inside the cohesive zone at these two velocities.

The variation of the pure shear cohesive zone length (L_{c1}) with respect to the propagation velocity is shown in Fig. 3. The length of the cohesive zone is inversely proportional to the premultiplier C_1 in the subsonic regime and decreases monotonically up to the Rayleigh wave speed, at which the cohesive zone length vanishes. Steady-state crack propagation at velocities between the Rayleigh and shear wave speeds is not physical, since it would lead to a negative cohesive zone length. In the intersonic regime, crack

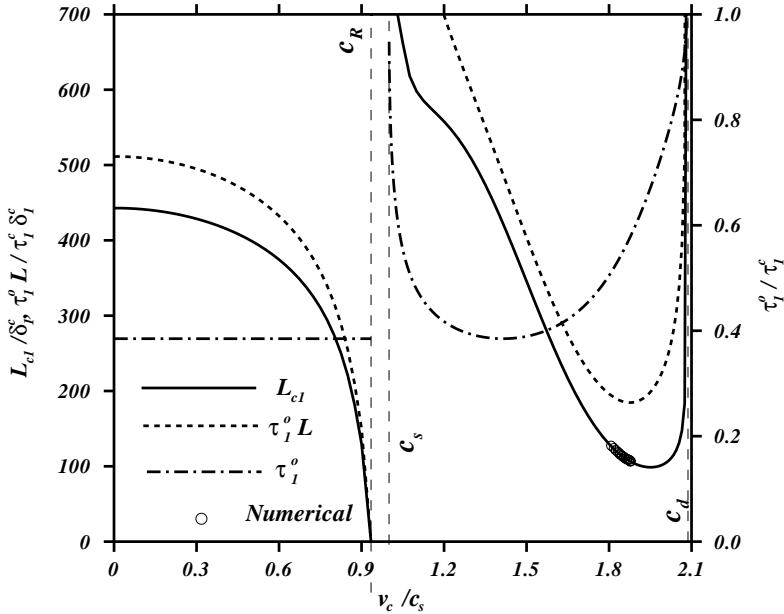


Fig. 3. Variation of the cohesive zone length L_{c1} , applied total external load $\tau_1^0 L$ and applied distributed load τ_1^0 with respect to the crack velocity v_c for the mode 2 case with $L = 3L_{c1}$. The symbols correspond to the length of the cohesive zone obtained for the follower load problem from the spectral simulations (Geubelle and Kubair, 2001) under quasi-steady-state conditions.

propagation at both the shear and dilatational wave speeds lead to an infinite cohesive zone length. The smallest cohesive zone length is attained at a velocity at which the premultiplier is maximum, i.e., at $v_c = 1.94c_s$. For comparison, quasi-steady-state cohesive zone lengths extracted from the numerical simulations performed for the same follower load problem with $L = 3L_{c1}$ using the spectral scheme (Geubelle and Kubair, 2001) are also plotted in Fig. 3, showing an excellent agreement.

The other two curves in Fig. 3 are concerned with the velocity dependence of the follower load τ_1^0 for the pure mode 2 case. The “dashed” curve corresponds to the total applied shear load $\tau_1^0 L$ normalized by $\tau_1^c \delta_1^c$, which is twice the fracture toughness of the material on the fracture plane. As before, the extent of the applied load L was set at three times the cohesive zone length L_{c1} . As apparent in Fig. 3, the variation of the total force with the crack speed is similar to that of the cohesive zone length, both in the subsonic and intersonic regimes. In the intersonic regime, the convex shape of the total applied shear load curve indicates the existence of an unstable region of crack propagation, thus favoring the higher of the two crack speeds possible for any given amplitude of the total applied load. The last curve in Fig. 3 shows the velocity variation of the amplitude of the applied distributed load τ_1^0 required to cancel the crack tip singularity, normalized by the cohesive strength τ_1^c . Due to the invariance of the order of singularity with respect to the velocity in the subsonic regime, the required distributed load remains constant. In the intersonic regime, however, the distributed

load curve has the same convex nature as the total shear load, but reaches a minimum (≈ 0.378) at a crack speed of $\sqrt{2}c_s$. Note that the magnitude of this minimum load is equal to that in the subsonic regime since the orders of singularity are the same ($q_1 = 1/2$). The various comments regarding the follower load τ_1^0 explain the limited range of the quasi-steady-state values of L_{c_1} obtained through the spectral scheme simulations of spontaneous crack motion (symbols in Fig. 3). As shown by Geubelle and Kubair (2001), intersonic crack motion is possible only when the distributed applied load τ_1^0 represents a substantial fraction (about 50%) of the cohesive strength. Therefore, for lower values of τ_1^0 , no intersonic crack motion was observed using the spectral scheme: the crack either propagates subsonically or remains stationary. For higher values of v_c approaching the dilatational wave speed c_d , the crack propagation becomes increasingly unsteady, preventing a comparison with the analytical solution.

4. Mixed mode crack propagation

In the subsonic regime, a combination of shear as well as tensile damage is responsible for crack propagation. This results in a smaller cohesive zone compared to either of the pure mode cases. The reduction in the cohesive zone length can be quantified by the ratio

$$A = \frac{L_c(v_c)}{L_{c_1}(v_c)}, \quad (35)$$

where L_c is the mixed mode cohesive zone length and L_{c_1} is the cohesive zone length obtained in mode 2, which serves as our reference case. Special emphasis is placed hereafter on problems characterized by predominantly shear loading ($\gamma \geq 45^\circ$) since, it has been shown by Geubelle and Kubair (2001) that only these cases lead to intersonic propagation. Variation of A with the propagation velocity is shown in Fig. 4 for different values of the loading mixity γ defined in (20). For lower velocities of propagation, significant tensile damage is present in the cohesive zone. For propagation velocities approaching the Rayleigh wave speed, a predominant shear failure inside the cohesive zone is evident even for a mode mixity of $\gamma = 45^\circ$. The length ratio A is finite at the Rayleigh wave speed, at which both the mixed mode and the mode 2 cohesive zone lengths vanish.

The length ratio Γ defined in Eq. (23) quantifies the relative extents of tensile and shear damage inside the cohesive zone and depends on both the propagation velocity v_c and the applied mode mixity γ (Fig. 4). For all values of γ , an increase in crack velocity leads to a relative reduction in the extent of the tensile damage in the cohesive zone. For example, when the applied distributed load has equal tensile and shear components ($\gamma = 45^\circ$), the value of Γ goes from 1 at $v_c = 0$ to approximately 0.1 at $v_c = c_R$. It has to be noted once again that for all mode mixities, the cohesive zone length tends to zero as v_c approaches c_R . The results presented in Fig. 5 indicate that, at crack speeds close to c_R , the tensile cohesive zone length reduces more rapidly than the shear component, leading to an increasingly shear dominated failure at these velocities.

The solution in the intersonic regime is illustrated in Fig. 6, which presents the spatial variations of the stress σ_{x2} and displacement jumps δ_x are shown for a velocity

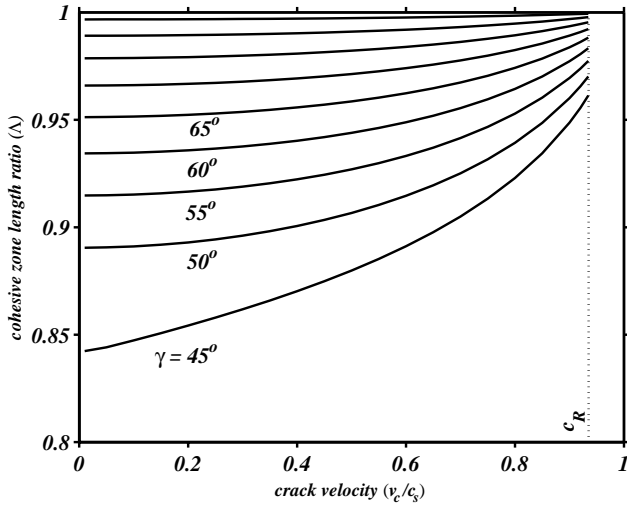


Fig. 4. Subsonic crack propagation under mixed-mode conditions: velocity dependence of ratio of the mixed-mode to pure shear cohesive zone length for various values of the loading mode mixity γ (shown in increments of 5° starting at 45°).

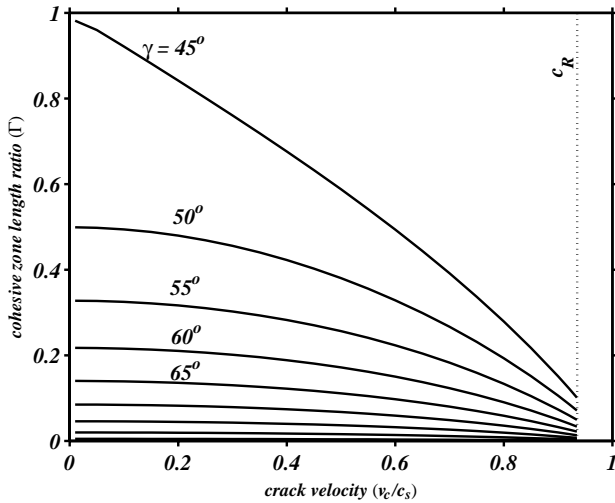


Fig. 5. Variation of the ratio of tensile cohesive zone length to the length of the mixed-mode cohesive zone L_{c2}/L_c , with respect to the crack propagation velocity v_c for various values of mode mixity γ . This figure illustrates the reduction of the tensile failure process as the crack speed and mode mixity increase.

$v_c = 1.5c_s$ and a remote mode mixity $\gamma = 55^\circ$. The solution depicted in the figure is for a distributed follower load τ^0 up to a distance $L = 3L_c$ behind the cohesive zone tip. As indicated in Section 2, the mixed-mode problem is decoupled due to the absence of the tensile damage inside the cohesive zone. As apparent from the figure,

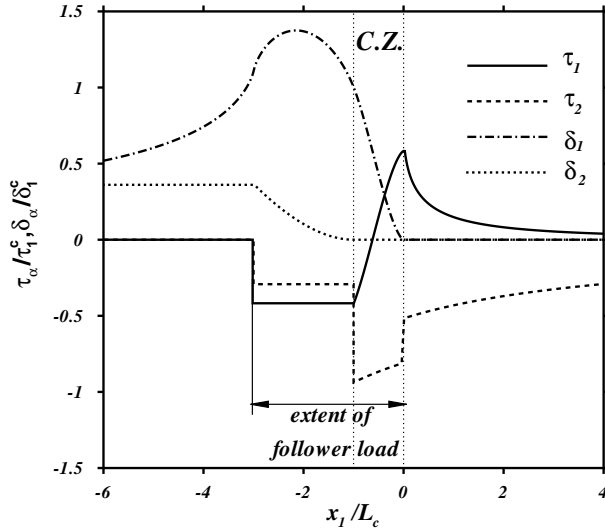


Fig. 6. Spatial variation of the stresses (τ_x) and displacement jumps (δ_x) on the crack plane for an intersonic crack speed $v_c = 1.5c_s$ and a remote mode mixity $\gamma = 55^\circ$. The solution is shown for a constant follower load τ^0 behind the cohesive zone tip up to a distance of $L = 3L_c$. The figure illustrates the absence of tensile damage inside the cohesive zone.

the shear traction τ_1 exhibits a stress concentration ahead of the cohesive zone tip and reaches a maximum at the cohesive zone tip which marks the beginning of the cohesive shear damage. The amplitude of this maximum is $\tau_1^c - \tau_1^0$, due to the applied traction boundary condition. Inter-sonic motion of a crack subjected to an externally applied tensile load leads to a compressive normal stress. Due to the applied traction τ_2^0 inside the cohesive zone, the normal stress distribution is discontinuous. Both tangential and normal tractions become equal to the externally applied traction behind the crack tip up to a distance L , beyond which the crack faces are traction free. The other two curves in Fig. 6 correspond to the spatial distribution of the crack displacement jumps δ_x . Crack sliding δ_1 begins at the cohesive zone tip and increases monotonically to δ_1^c at the crack tip owing to the Dugdale condition. Due to the finiteness of the externally applied distributed load, the crack sliding displacement reduces behind the crack tip. Due to the absence of the tensile cohesive damage, the crack only begins to open at the crack tip and increases monotonically up to a distance L behind the cohesive zone tip, beyond which the crack opening remains constant since the opening slope $\delta_2' = 0$ (Eq. (27)).

Once the solution for δ_x , δ_z and τ_x is known in the cohesive zone the stress distribution in the (x_1, x_2) plane can be computed from analytical continuation of the complex functions F and G . In Fig. 7, contours of the maximum shear stress τ_{max} are shown for two representative velocities $v_c = 0.8c_s$ and $v_c = 1.6c_s$, and for a remote mixity angle $\gamma = 45^\circ$. Away from the cohesive zone, the subsonic contours have a three-lobed pattern resembling a pure mode 1 photoelastic fringe pattern rotated by the mixity angle, even

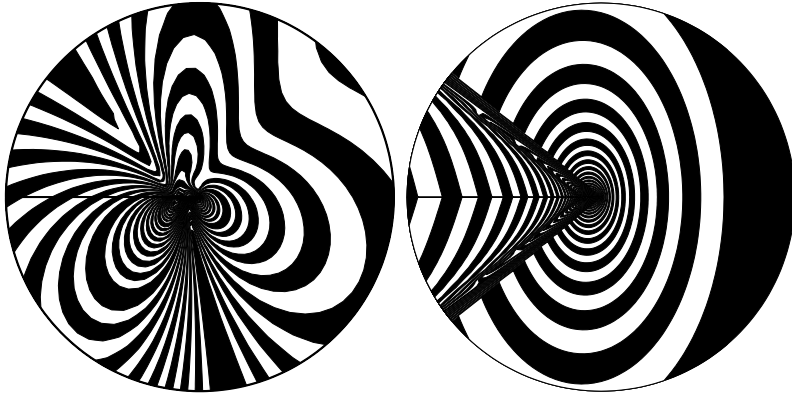


Fig. 7. Contours of the maximum shear stress for a loading mixity of 45° and propagation velocities $v_c = 0.8c_s$ (left) and $1.6c_s$ (right). The contours are shown up to an outer radius $R = 10 \times L_c$ around the cohesive zone tip.

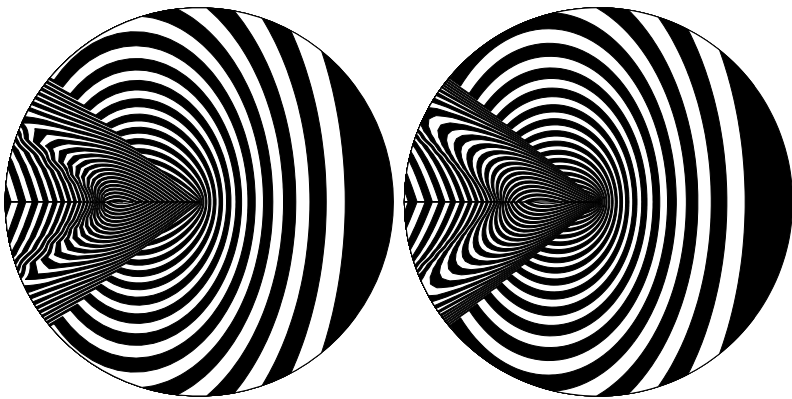


Fig. 8. Comparison of the near tip fringes for two mode-mixities: $\gamma = 45^\circ$ (left) and 90° (right) for a propagation velocity $v_c = 1.6c_s$. The figure illustrates the difference between the mixed-mode and pure shear loadings associated with the presence of a weak shear shock in the mixed-mode case emanating from the crack tip. The contours are shown up to an outer radius $R = 2 \times L_c$ around the cohesive zone tip.

though a predominantly shear failure process is operative inside the cohesive zone. In the intersonic case, however, the fringe pattern is similar to that obtained for a pure shear loading (Samudrala et al., 2002).

Finally, the near-tip details of the intersonic fringe pattern shown in Fig. 8 illustrate the difference between the pure shear and mixed-mode cases, as indicated by the shear shock like structure emanating from the crack tip in the mixed-mode case (left) due to the superposition of the tensile field, which is evidently absent in the pure shear case (right).

5. Conclusions

We can summarize the results from the mixed-mode case as follows:

1. In the subsonic regime, the mixed-mode cohesive zone length is smaller in comparison with the pure mode cases and depends both on the propagation velocity as well as on the applied mode-mixity.
2. A combination of tensile and shear cohesive failure is responsible for subsonic propagation under predominantly shear mixed-mode loading conditions. Significant tensile damage can be observed at smaller crack speeds, but the failure becomes shear-dominated as the crack speed approaches the Rayleigh wave speed.
3. Only shear damage is present inside the cohesive zone in the intersonic regime. As a result of the applied tensile loading, crack opening is observed only behind the crack tip.

Acknowledgements

Part of this work has been supported by the ASCI Center for the Simulation of Advanced Rockets funded by the US Department of Energy through the University of California under subcontract number B341494. Y.H. acknowledges the support from ONR (grant N00014-01-1-0205, program monitor Dr. Y.D.S. Rajapakse).

Appendix A. Closed-form solution

The closed-form solution to Eqs. (9) and (15) with a spatially dependent cohesive law of the form $\tau_\alpha = \tau_\alpha^c(1 - x_1/L_{c_\alpha})$ is summarized here for the pure mode cases. This solution has been used in the present study to validate the numerical quadrature scheme. In this appendix, $\alpha = 1$ corresponds to mode 2 case and $\alpha = 2$ represents the mode 1 case. No summation is assumed on α .

For the problem of a distributed follower load τ_α^0 applied up to a distance $L = bL_{c_\alpha}$ behind the cohesive zone tip, the solution in the subsonic regime is given by

$$\begin{aligned} \frac{\pi}{2C_\alpha} \frac{\mu}{\tau_\alpha^c} \delta'_\alpha(\hat{x}) &= (1 - \hat{x}) \tanh^{-1} \left(\frac{1}{\sqrt{\hat{x}}} \right) + \sqrt{\hat{x}} - \frac{2}{3\sqrt{b}} \tanh^{-1} \left(\sqrt{\frac{b}{\hat{x}}} \right), \\ \frac{\pi}{2} \frac{\sigma_{\alpha 2}(\hat{x})}{\tau_\alpha^c} &= (1 + \hat{x}) \tan^{-1} \left(\frac{1}{\sqrt{\hat{x}}} \right) - \sqrt{\hat{x}} - \frac{2}{3\sqrt{b}} \tan^{-1} \left(\sqrt{\frac{b}{\hat{x}}} \right), \\ \frac{\pi}{C_\alpha} \frac{\mu}{\tau_\alpha^c} \frac{\delta_\alpha(\hat{x})}{L_{c_\alpha}} &= (1 + \hat{x})\sqrt{\hat{x}} - (1 - \hat{x})^2 \tanh^{-1} \left(\frac{1}{\sqrt{\hat{x}}} \right) \\ &\quad + \frac{4(b - \hat{x})}{3\sqrt{b}} \tanh^{-1} \left(\sqrt{\frac{b}{\hat{x}}} \right) - \frac{4}{3} \sqrt{\hat{x}}, \end{aligned} \quad (\text{A.1})$$

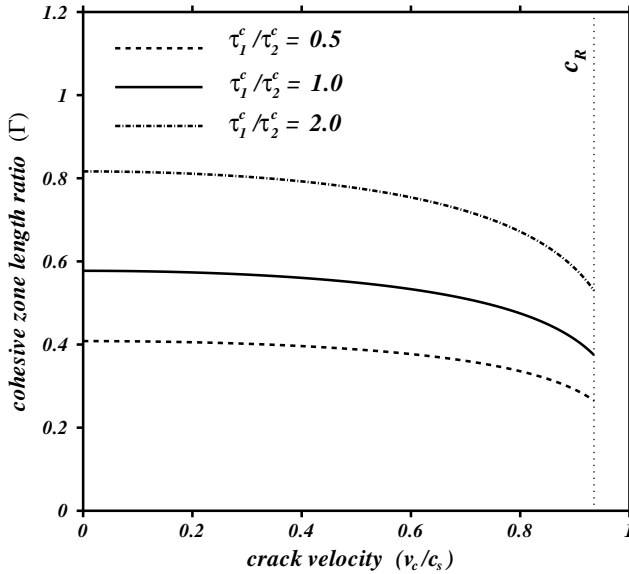


Fig. 9. Variation of the ratio of tensile cohesive zone length to the length of the mixed-mode cohesive length L_{c2}/L_c (B.2), with respect to the crack propagation velocity v_c for a mode-mixity $\gamma=60^\circ$. This figure illustrates the effect of varying the ratio of cohesive strengths in tension and shear.

where $\hat{x} = x_1/L_{c_x}$. A stress intensity factor based loading can be extracted from Eq. (A.1) setting $b = \infty$.

Appendix B. Expression of Γ

For the spatially varying cohesive law introduced in Appendix A, the length ratios Γ and Λ defined by Eqs. (23) and (35) can be written as

$$\int_0^{\Lambda-(1-\Gamma)} \frac{\tau(\eta + (1 - \Gamma))}{\sqrt{\eta}} d\eta = \sqrt{\cot^2(\gamma) \frac{\alpha_s}{\alpha_d} \frac{\tau_1^c}{\tau_2^c} \frac{\delta_2^c}{\delta_1^c}} \int_0^\Lambda \frac{\tau(\eta)}{\sqrt{\eta}} d\eta. \tag{B.1}$$

With $\tau_1 = \tau_2 = \tau^c(1 - x_1/L_c)$, Eq. (B.1) yields $\Lambda = 1$ and

$$\Gamma = \sqrt{\cot^2(\gamma) \frac{\alpha_s}{\alpha_d} \frac{\tau_1^c}{\tau_2^c} \frac{\delta_2^c}{\delta_1^c}}. \tag{B.2}$$

Relation (B.2) allows us to quantify the influence of the shear to tensile strength ratio (τ_1^c/τ_2^c) on the relative importance of normal and tangential cohesive failure. The variation of Γ with respect to the crack speed is illustrated in Fig. 9 for three values of τ_1^c/τ_2^c . As expected, when the shear strength τ_1^c exceeds the tensile strength τ_2^c , normal failure plays a more important role in the overall failure process, thereby reducing Γ . The opposite is true when $\tau_1^c < \tau_2^c$.

References

- Breitenfeld, M.S., Geubelle, P.H., 1998. Numerical analysis of dynamic debonding under 2D in-plane and 3D loading. *Int. J. Fracture* 93, 13–38.
- Broberg, K.B., 1980. Velocity peculiarities at slip propagation. Brown University Report.
- Broberg, K.B., 1989. The near-tip field at high crack velocities. *Int. J. Fracture* 39, 1–13.
- Burridge, R., 1973. Admissible speeds for plane-strain self-similar shear cracks with friction but lacking cohesion. *Geophys. J. Roy. Astron. Soc.* 35, 439–455.
- Burridge, R., Conn, G., Freund, L.B., 1979. The stability of a plane strain shear crack with finite cohesive force running at intersonic speeds. *J. Geophys. Res.* 84, 2210–2222.
- Erdogan, F., Gupta, G.P., Cook, T.S., 1973. Numerical solution of singular integral equations. In: *Mech. Frac.* 1, Sih (Ed.), Nordhoff 77, 368–425.
- Freund, L.B., 1979. The mechanics of dynamic shear crack propagation. *J. Geophys. Res.* 84, 2199–2209.
- Freund, L.B., 1990. *Dynamic Fracture Mechanics*. Cambridge University Press, Cambridge.
- Gao, H., Huang, Y., Gumbsch, P., Rosakis, A.J., 1999. On radiation-free transonic motion of cracks and dislocations. *J. Mech. Phys. Solids* 47, 1941–1961.
- Geubelle, P.H., Kubair, D.V., 2001. Inter-sonic crack propagation in homogeneous media under shear-dominated loading: numerical analysis *J. Mech. Phys. Solids* 49, 571–587.
- Geubelle, P.H., Rice, J.R., 1995. A spectral method for 3D elastodynamic fracture problems. *J. Mech. Phys. Solids* 43, 1791–1824.
- Huang, Y., Gao, H., 2001. Inter-sonic crack propagation. Part I: the fundamental solution *ASME J. Appl. Mech.* 68, 169–175.
- Huang, Y., Gao, H., 2002. Inter-sonic crack propagation. Part II: suddenly stopping crack. *ASME Trans J. App. Mech.* 69, 76–80.
- Ravi-Chandar, K., Lu, J., Yang, B., Zhu, Z., 2000. Failure mode transitions in polymers under high strain rate loading. *Int. J. Fracture* 101 (1–2), 33–72.
- Rosakis, A.J., Samudrala, O., Coker, D., 1999. Cracks faster than shear wave speed. *Science* 284, 1337–1340.
- Samudrala, O., Huang, Y., Rosakis, A.J. 2002. Subsonic and inter-sonic shear rupture of weak planes with a velocity weakening cohesive zone. *J. Geophys. Res.* in press.